AFRL-AFOSR-UK-TR-2011-0049

Low Strain Rate Failure of Compliant Flexures

Matthew J Santer

Imperial College London
Department of Aeronautics
Prince Consort Road
London, United Kingdom SW7 2AZ

EOARD GRANT 10-3065

October 2011

Final Report for 29 April 2010 to 29 June 2011

Air Force Research Laboratory
Air Force Office of Scientific Research
European Office of Aerospace Research and Development
Unit 4515 Box 14, APO AE 09421

REPORT DOCUMENTATION PAGE

Form Approved OMB No. 0704-0188

1. REPORT DATE *(DD-MM-YYYY)*	2. REPORT TYPE	3. DATES COVERED *(From – To)*
06-10-2011	Final Report	29 April 2010 – 29 June 2011

4. TITLE AND SUBTITLE

Low Strain Rate Failure of Compliant Flexures

5a. CONTRACT NUMBER

FA8655-10-1-3065

5b. GRANT NUMBER

Grant 10-3065

5c. PROGRAM ELEMENT NUMBER

6. AUTHOR(S)

Dr. Matthew J. Santer

5d. PROJECT NUMBER

5d. TASK NUMBER

5e. WORK UNIT NUMBER

7. PERFORMING ORGANIZATION NAME(S) AND ADDRESS(ES)

Imperial College London
Department of Aeronautics
Prince Consort Road
London, United Kingdom SW7 2AZ

8. PERFORMING ORGANIZATION REPORT NUMBER

N/A

9. SPONSORING/MONITORING AGENCY NAME(S) AND ADDRESS(ES)

EOARD
Unit 4515 BOX 14
APO AE 09421

10. SPONSOR/MONITOR'S ACRONYM(S)

AFRL/AFOSR/RSW (EOARD)

11. SPONSOR/MONITOR'S REPORT NUMBER(S)

AFRL-AFOSR-UK-TR-2011-0049

12. DISTRIBUTION/AVAILABILITY STATEMENT

Approved for public release; distribution is unlimited. (approval given by local Public Affairs Office)

13. SUPPLEMENTARY NOTES

14. ABSTRACT

This project investigates the time-dependent properties of thin carbon fiber composite flexures when they are held in a folded (stowed) configuration for long periods of time. The resulting behavior is shown to be complex and time dependent in an experimental program to determine the full field strain and evolution of microstructural damage. The program uses a developed experimental rig which uses digital image correlation to measure the strain behavior over long time durations. Possible numerical analyses to capture the observed responses are considered. It is concluded that an understanding of the microstructural and probabilistic behavior is crucial to the understanding of long term flexure properties.

15. SUBJECT TERMS

EOARD, microstructural damage, carbon fiber composite flexures

16. SECURITY CLASSIFICATION OF:			17. LIMITATION OF ABSTRACT	18, NUMBER OF PAGES	19a. NAME OF RESPONSIBLE PERSON
a. REPORT	b. ABSTRACT	c. THIS PAGE			Brad Thompson
UNCLAS	UNCLAS	UNCLAS	SAR	28	19b. TELEPHONE NUMBER *(Include area code)* +44 (0)1895 616163

Low Strain Rate Failure of Compliant Flexures: Final Report

Dr. M. Santer
Department of Aeronautics
Imperial College London
Prince Consort Road
London, SW7 2AZ, UK
email: m.santer@imperial.ac.uk

Contents

1 Summary **5**

2 Introduction **5**
2.1 DIC Rig Development 5
2.2 Digital Image Correlation (DIC) 7
2.3 High Strain Rate Compression Testing 8

3 Low Strain Rate Behavior of Compliant Flexures – Experimental Program **11**
3.1 Experimental Procedure 11
3.2 Temperature and Humidity Variation 13
3.3 Strain Evolution 13
3.4 Microscopy and Damage Evolution 16
3.5 Experimental Program – Conclusions 19

4 Low Strain Rate Behavior of Compliant Flexures – Numerical Modelling **21**
4.1 Finite Element Modelling and Analysis 21
4.2 Viscoelastic Material Hypothesis 22
4.3 Numerical Modelling – Conclusions 23

5 General Conclusions **25**
5.1 Future Work 25

List of Figures

Figure 1: Long-term bending rig in its 2D strain field measurement configuration

Figure 2: Compressive force vs. platen separation for UD IM7-8552 2 ply, 3 ply, and 4 ply specimens

Figure 3: Illustration of DIC imaging of the tensile surface of a 3-ply specimen immediately after bending, and after two weeks

Figure 4: The variation of temperature and humidity during the experiment duration showing relative consistency and day/night variation

Figure 5: Measured principal strain changes on the line of highest curvature represented by the mean over four equal regions

Figure 6: Average principal strain evolution for all experimental specimens

Figure 7: Example microscope images of deformed specimen

Figure 8: Illustration of image comparison to determine damage evolution

Figure 9: Schematic diagrams showing the time of appearance of crack damage in the region of highest curvature of all test specimens

Figure 10: Finite element analysis showing the maximum principal strain on the tensile surface of a 2 ply specimen

Declarations

I assure that an acknowledgement of Government support will appear in any publication of any material based on or developed under this project, in the following terms: 'Effort sponsored by the Air Force Office of Scientific Research, Air Force Material Command, USAF, under grant number FA8655-10-1-3056. The U.S. Government is authorized to reproduce and distribute reprints for Government purpose notwithstanding any copyright notation thereon.'

The views and conclusions contained herein are those of the author and should not be interpreted as necessarily representing the official policies or endorsements, either expressed or implied, of the Air Force Office of Scientific Research or the U.S. Government.

I certify that there were no subject inventions to declare during the performance of this grant.

1 Summary

This project investigates the time-dependent properties of thin carbon fiber composite flexures when they are held in a folded (stowed) configuration for long periods of time. The resulting behavior is shown to be complex and time dependent in an experimental program to determine the full-field strain and evolution of microstructural damage. The program uses a developed experimental rig which uses digital image correlation to measure the strain behavior over long time durations. Possible numerical analyses to capture the observed responses are considered. It is concluded that an understanding of the microstructural and probabilistic behavior is crucial to the understanding of long term flexure properties.

2 Introduction

The use of compliant fiber-composite flexures in deployable space structures enables the design of systems that are both lightweight and exhibit high packaging ratios [4]. Large localized deformation in bending, instead of using conventional mechanism components such as hinges, allows the structures to be stowed for launch. Their quasi-static behavior is reasonably well characterized by the assumption of linear orthotropic material properties and either an analytical approach – such as Euler's elastica [7] – or a geometrically-nonlinear finite element analysis. These methods, however, are currently unable to predict the behavior of compliant flexures with accuracy when time-dependent effects cannot be neglected.

Time-dependence is of crucial importance at two points in the typical operational life of a compliant flexure. One is the high rate regime during deployment in which stored strain energy is rapidly released resulting in shock loading. The second – the focus of this experimental program – is the low rate regime when the flexures are in their stowed configuration. In this case viscoelastic, viscoplastic, and other time-dependent phenomena can result in the properties of the flexure changing over relatively long time durations. In relatively benign cases this can result in dissipation of strain energy required to self-deploy and a lack of positional accuracy when deployed. In more critical cases, apparently stably-stowed structures can suddenly fail. In this program compliant flexures are tested to determine their long-term behavior using a developed digital image correlation (DIC)-based rig.

For the remainder of this introductory section, key developments which have already been discussed in the interim report, but which nonetheless form a necessary precursor to the main experimental effort, are recapped.

2.1 DIC Rig Development

The developed DIC strain measurement rig for the simultaneous long-term characterization of the response of multiple flexures was introduced in the interim report. An operating procedure is also provided. However, the rig design is summarized here for convenience.

The developed long-term bending experimental rig is shown in Fig. 1. The rig is shown in its 2D strain field measurement configuration with a single SLR camera. This rig has two distinct functions: the first is to provide a means to bend thin composite flexures under displacement control

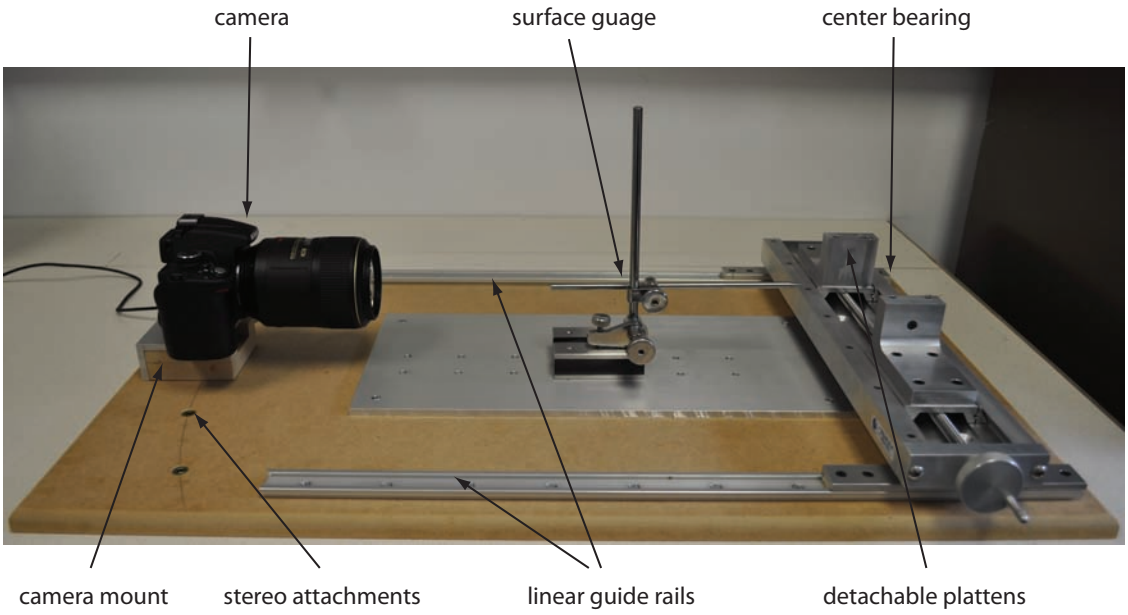

Figure 1: Long-term bending rig in its 2D strain field measurement configuration

in a repeatable manner; the second is to provide a stable platform to enable DIC measurements to be carried out.

In the following, italicized text refers to a label in Fig. 1. The displacement-controlled bending is carried out using the *center bearing* shown. This consists of two guided platforms which are connected to two screw threads, one left-hand thread and one right-hand thread with minimal backlash. Attached to these guided platforms are two angled sections which serve as attachment points for the *detachable platens*. These platens are the surfaces that compress the test specimen. The use of their detachability and the additional locking components – which enable both sides of the test specimen to be imaged – is demonstrated in the following section. As the driving handle is rotated the platens move together towards a fixed center line. This fixed line forms a reference for the DIC images.

A fixed point in space is provided by the *surface gauge* which consists of a pointer mounted on a rigid plate. At any stage of folding, the centered test specimen may be returned to the same location by moving the center bearing on the *linear guide rails* until the specimen touches the surface gauge pointer. This provides a fixed frame of reference for the DIC imaging and enables the same rig to be used to test multiple specimens over the same time duration.

For 2D strain field measurement, a single SLR camera is required as shown. The camera is a Nikon D-60 10.2 MPix (CCD size 23.6 mm $\times$ 15.8 mm) with a Nikkor 105 mm f/2.8 lens. The lens is chosen to maximize the resolution over the 50 mm $\times$ 50 mm region of interest. The camera is secured to the rig by means of an adjustable *camera mount*. For stereo imaging to enable 3D DIC additional *stereo attachment* points are provided to enable a second identically-configured camera to be mounted. The cameras are remotely controlled via a PC running the NKRemote commercial software package.

2.2 Digital Image Correlation (DIC)

The consistent repeatable location of both sides of multiple test specimens provided by the developed rig enables DIC full field strain analysis to be carried out. The DIC is carried out using the MatchID software [2] developed at the University of Gent. The advantages of this software are that it provides high, and importantly quantifiable, accuracy and offers multiple correlation algorithms. Its disadvantage is that it is slow when compared to its commercial equivalents. This, however, is not a substantial problem for this program as real-time data processing is not required.

In this case, the test specimens are speckled using silver glitter spray paint as this was found to be the process that gave the best size and distribution of speckles at the required resolution. The downside to using metallic speckles is that direct lighting can lead to glare which reduces the quality of the DIC. An additional problem concerns the observation of the compressive surface as light is restricted by the specimen itself. To overcome these difficulties, strong diffuse lighting is used and images are converted to greyscale before processing. This conversion also has the advantage of significantly speeding up the correlations.

Of the many available options available in MatchID, the correlation algorithm that gave best results for the bent specimens was found to be the Approximated Normalized Sum of Square Differences (ApproxNSSD). In this case an optimization process is used to minimize the coefficient

$$r_{SSD} = 1 - \frac{\sum_y \sum_x [f(x,y) - g[\mu(x,y,\mathbf{s}), \nu(x,y,\mathbf{s})]]^2}{\sum_y \sum_x f^2(x,y)} \tag{1}$$

in which the Hessian is approximated as

$$\frac{\partial^2 C}{\partial s_i \partial s_j} \approx \frac{2}{\sum_y \sum_x f^2} \sum_y \sum_x \frac{\partial g}{\partial s_i} \frac{\partial g}{\partial s_j} \tag{2}$$

which enables point correspondences between the images to be determined. Accurate determination of sub-pixel displacements is carried out via bi-cubic interpolation. The 2D deformation is currently approximated as an affine transformation

$$\begin{bmatrix} \mu(x,y,\mathbf{s}) \\ \nu(x,y,\mathbf{s}) \end{bmatrix} = \begin{bmatrix} x \\ y \end{bmatrix} + \begin{bmatrix} u \\ v \end{bmatrix} + \begin{bmatrix} \frac{\partial u}{\partial x} & \frac{\partial u}{\partial y} \\ \frac{\partial v}{\partial x} & \frac{\partial v}{\partial y} \end{bmatrix} \begin{bmatrix} \Delta x \\ \Delta y \end{bmatrix} \tag{3}$$

which is found to provide an accurate representation.

Having determined the deformation field the deformation gradient $\mathbf{F}$ may be determined. From this, the strain tensor field may be deduced using standard formulae. The most informative results for this particular problem have been observed to be the Green-Lagrange tensor

$$\mathbf{E}_{(G-L)} = \frac{1}{2}(\mathbf{C} - \mathbf{I}) \tag{4}$$

and Euler-Almansi tensor

$$\mathbf{E}_{(E-A)} = \frac{1}{2}(\mathbf{I} - \mathbf{c}) \tag{5}$$

in which $\mathbf{C} = \mathbf{F}^T\mathbf{F}$ is the right Cauchy-Green deformation tensor, and $\mathbf{c} = \mathbf{F}^{-T}\mathbf{F}^{-1}$ is the left Cauchy-Green deformation tensor.

The main complexity in the 2D DIC analysis that is carried out is determining the region of the image over which it is valid to carry out the correlation i.e. the region over which the deformed

sample remains sufficiently flat in the vicinity of the maximum curvature. It is possible to determine this approximately by close inspection of the images. However, to maximize accuracy, results are recorded for the line along the region of highest curvature only.

2.3 High Strain Rate Compression Testing

In this section, a brief summary of the high-rate bending response testing is presented. This has already been discussed in the interim report, but it is recapped here as the tests are a necessary precursor to the long-duration tests. The purpose of these short-term (high-rate) bending tests is to:

1. validate the work presented in Murphey et al. [6, 3] which forms the basis for the proposed long-term response testing;
2. validate the requirement to reduce test specimen length;
3. validate the specimen manufacture process;
4. determine a lower bound for material characteristic response time;
5. carry out preliminary fractographic studies.

The compression-bending testing is carried out in an Instron electro-mechanical universal testing machine with a 1 kN load cell. Displacement is measured using the in-built screw gage. The specimen is placed between two lipped platens which are set initially at a separation of 2 mm less than the specimen length. This is to ensure that the specimen is adequately gripped before the testing commences. The platens are then brought together at a rate of 12 mm/min. This rate is varied for some tests to 6 mm/min and 4 mm/min respectively for some specimens to address objective 4 above. The test is concluded when either the specimen is deemed to have failed, or when the platens reach a separation of 6 mm. Fractographic analysis has been carried out using high-power optical microscopes.

Bending tests were carried out for CFRP samples manufactured from IM7-8552 UD pre-preg. with 2, 3, and 4 plies. Specimens consisting of single plies were also constructed, but it was found to be impossible to carry out repeatable tests in the Imperial College facilities due to their fragility. The reacted load versus platen separation for the test specimens is plotted in Fig. 2. It can be seen that the response of the specimens has three characteristic regions. The first region runs from the start of the test to the point at which the platen surface makes contact with the specimens away from the ends. In this region, the specimen is undergoing simple Euler-type compression.

When the platen separation reduces below approximately 70 mm the second region begins and the load begins to increase. The specimen stiffness increases throughout the region until the first fiber breaks and the stiffness of the specimen begins to be compromised. This marks the beginning of the third and final region which is characterised by a gradual reduction in stiffness and complete failure occurs. This behavior matches the results presented by Murphey et al. [6, 3] both qualitatively and quantitatively. It has been observed that the Imperial College data has a much narrower spread than the AFRL data. The reason for this is that the tests were all commenced from an initially-straight configuration and the specimens were therefore subjected to an identical loading regime throughout the experiment. The close spread in data means that it is valid to use these results to determine the loading during the displacement-controlled long-term tests. The consistency also validates the specimen manufacture technique.

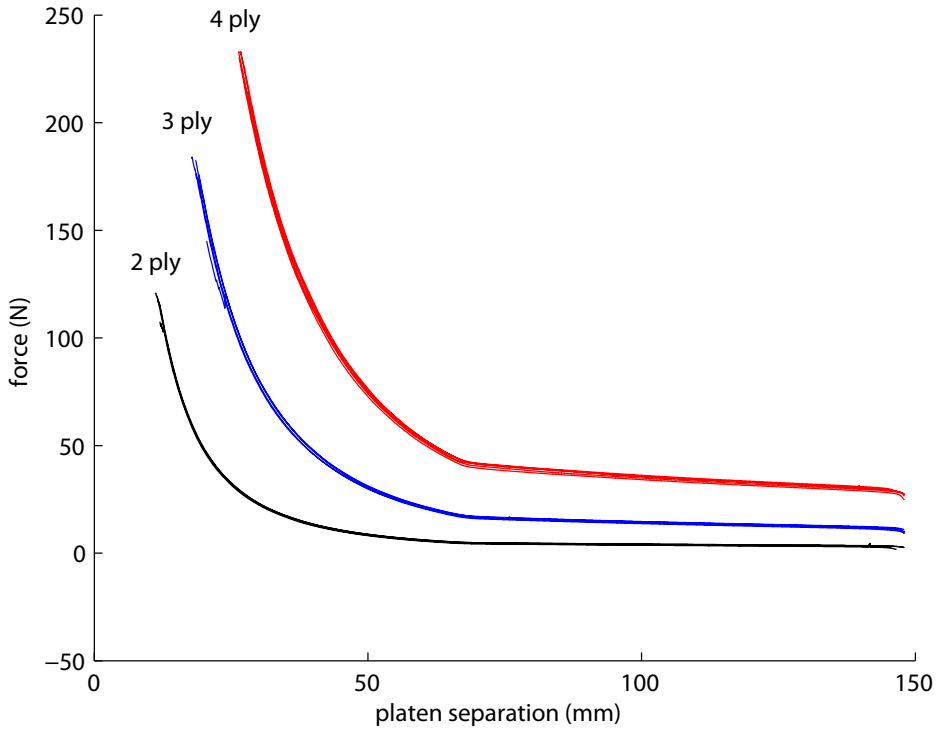

Figure 2: Compressive force vs. platen separation for UD IM7-8552 2 ply, 3 ply, and 4 ply specimens

Due to constraints placed by the lenses of the DIC system in the long-term test rig it was required to reduce the length of the test specimens from the 200 mm specified in Murphey et al. to 150 mm. It is necessary to show that this change in geometry has no effect on the structural performance. This was found to be the case – observed variability between the specimens of both lengths was no different to the variability between specimens of the same length. This is to be expected as the test method essentially means that the regions of the specimen that are in direct contact with the platens do not contribute to the structural response. It was also noted that there was no discernable difference in the structural response between loading at 12 mm/min and 4 mm/min. This is a valuable result: provided displacement is imposed at a rate faster than at least 4 mm/min it is not important to monitor the exact rate of compression of specimens in the long-term flexure tests, as viscoelastic effects will not have time to manifest themselves.

*

Following this introductory section, the remainder of this report describes the primary achievements of this research program: the results of the long-term experimental testing of IM7-8552 thin flexures using the developed test rig. Selected results will be presented which illustrate the resulting capability to capture the full-field strain response of the specimen surfaces in the region of maximum curvature. For long-term characterization of the global structural response, however, it is more illustrative to condense the strain to a single mean value. Results of this strain evolution are presented for all the 2, 3, and 4-ply specimens tested.

The full-field response is more usefully considered at a local scale. To facilitate this, high magnification microscope images are taken of the tensile surface of the flexures throughout the experimental

program. These are used to determine a microstructural damage evolution profile which may be correlated with the strain evolution data. Finally, a description of accompanying numerical analysis is provided, conclusions are drawn, and suggestions for further work are presented.

3 Low Strain Rate Behavior of Compliant Flexures – Experimental Program

The DIC-based experimental rig has been used to determine the long-term response of 9 IM7-8552 UD flexures, three each of $[0_n]$ where $n = 2, 3, 4$, over a period of 54 days. In this section the experimental procedure is elaborated. Following this, the effect of temperature and humidity variation is discussed. The experimentally-determined strain evolution in the region of highest curvature of the specimens is presented. In addition to the DIC strain measurement, the specimens are imaged under a high-power microscope and the evolution of localized damage is recorded. Conclusions regarding the experimental results are then drawn.

3.1 Experimental Procedure

In this section the long-term flexure test procedure is elaborated. Each test specimen is compressed under displacement control to a platen separation of 80% of the failure separation as determined by the short-term compression tests described above in Sec. 2.3. Although it is impossible to know prior to carrying out the experiment that this will be sufficient to instigate the time dependent effects that have been previously observed, this imposed deformation was found to be satisfactory.

Strain measurements are taken of both tensile and compressive surfaces immediately following compression, and subsequently at approximately seven day intervals initially. This was increased to approximately three day intervals when the strain was observed to be changing more rapidly after approximately 30 days. As a characteristic example of the measurements being taken, the principal Euler-Almansi strain measurements on the tensile surface of one of the $[0_3]$ specimens, determined by the DIC immediately after bending, and the change in strain in the same specimen after two weeks, are shown in Fig. 3.

As the most highly-curved region is difficult to determine a priori, it can be seen that a large rectangular correlation window has been selected including areas where the correlation is highly inaccurate due to the presence of out-of-plane deformation. Accurate measurement is restricted to the approximately planar region indicated by the dashed rectangle in Fig. 3 a. However, the strain values along the center line corresponding to the region of highest curvature are known to be the most accurate, and consequently are recorded. This is sufficient to allow meaningful assessment of the evolution of the values. The image correlation is carried out according to the settings elaborated in Sec. 2.2. The correlation subset window was set to a square of 25 pixels.

Immediately following the imaging of the specimens for DIC purposes, the tensile surfaces of the specimens are examined under a high-power microscope. The close separation of the compression platens means that the compressive surface is inaccessible to the microscope lens. Sequential images are compared in order to determine the evolution of damage. It is worth noting that one of the 2-ply specimens was additionally compressed to 90% of the failure separation after 21 days. This specimen failed spontaneously after 10 minutes, which is indicative of the degradation undergone by the deformed flexures.

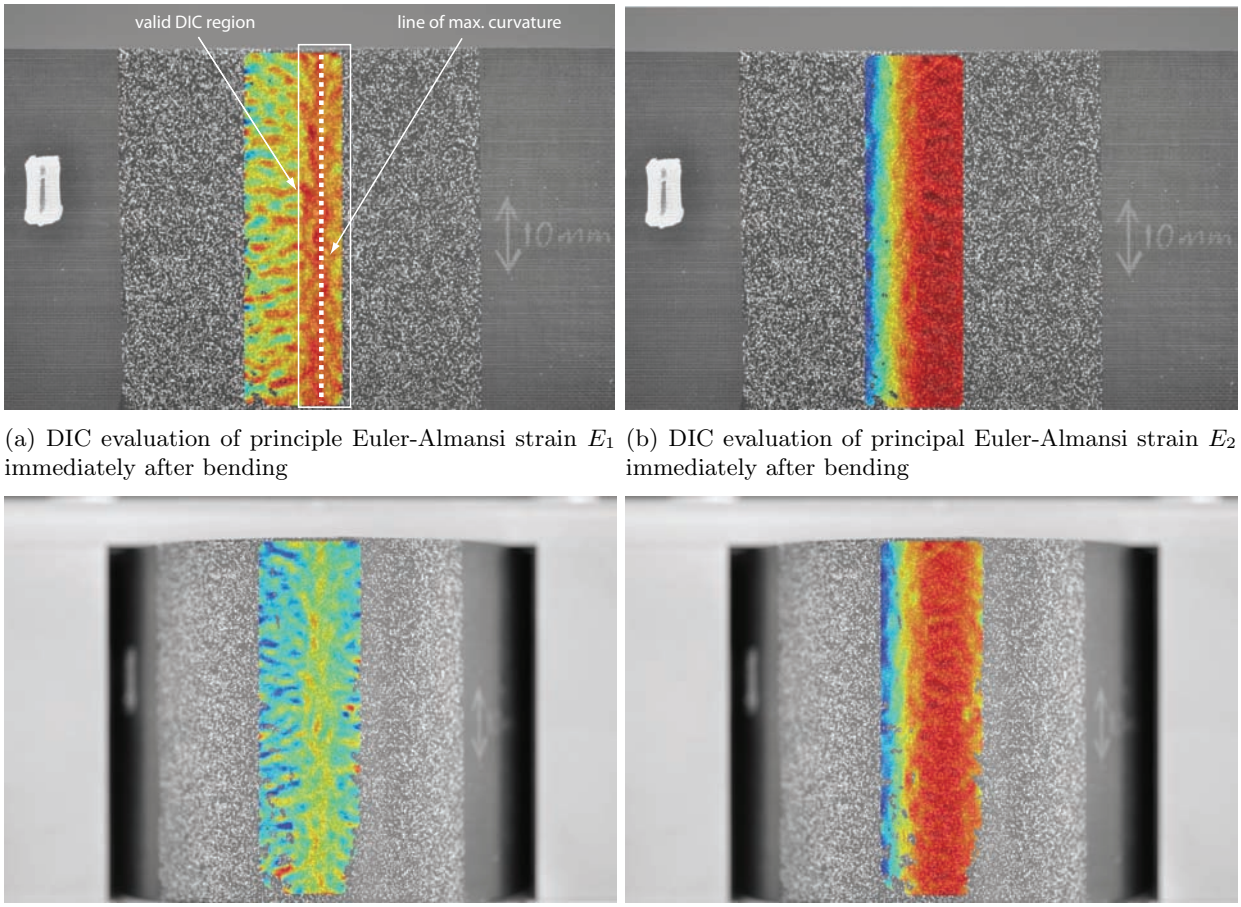

(a) DIC evaluation of principle Euler-Almansi strain E_1 immediately after bending

(b) DIC evaluation of principal Euler-Almansi strain E_2 immediately after bending

(c) DIC evaluation of change in E_1 after being held compressed for 2 weeks

(d) DIC evaluation of change in E_2 after being held compressed for 2 weeks

Figure 3: Illustration of DIC imaging of the tensile surface of a 3-ply specimen immediately after bending, and after two weeks. A scale is not provided as correlation is only meaningful in the region of highest curvature.

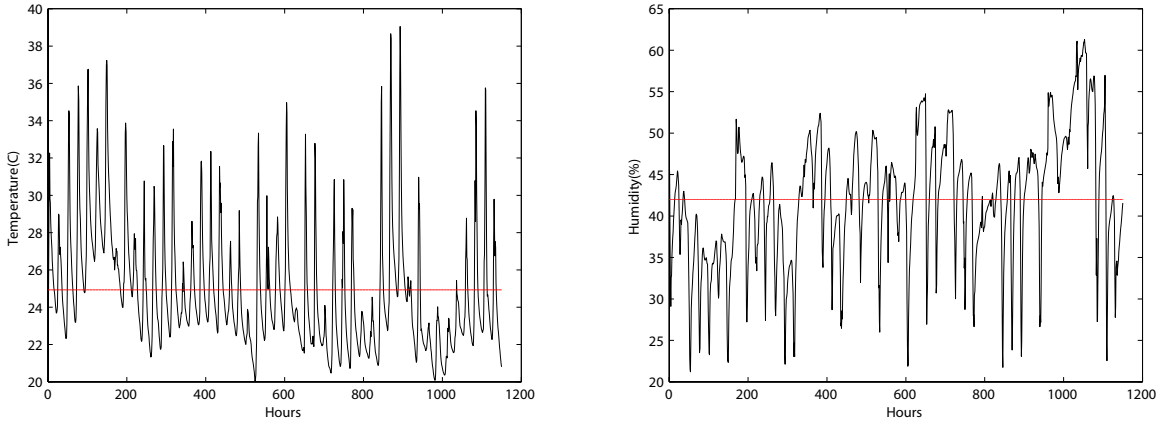

(a) Variation of temperature ($^{\circ}C$) over experiment duration

(b) Variation of relative humidity (%) over experiment duration

Figure 4: The variation of temperature and humidity during the experiment duration showing relative consistency and day/night variation. The mean values are shown with a dotted line.

3.2 Temperature and Humidity Variation

All test specimens were stored in the same location when not being imaged for DIC or under the microscope. Hourly readings of local temperature and humidity were taken to determine whether this had a significant effect on the measured specimen behavior. The temperature and humidity variations are plotted in Fig. 4. It can be seen that there is consistent day/night variation, but limited change over the duration of the experiment. The mean temperature is determined to be 24.9°C with a standard deviation of 3.3°C. The mean relative humidity was determined to be 42.0% with a standard deviation of 7.7%.

The variation occurs at a substantially higher rate than the observed variation in structural response. No correlation between this data and the strain evolution has been determined. It can therefore be concluded that temperature and humidity effects do not pay a significant role in the observed structural behavior.

3.3 Strain Evolution

As described above, digital image correlation (DIC) was used to determine the evolution of strain along the line of highest curvature of the bent test specimens. It was noted that the measurements were locally noisy; this is attributed to small variations in the ambient lighting, and the surface reflectivity of the test specimens. To overcome this noise and to enable better determination of the evolution of the strain profile over time, the strain measurements are averaged along the centreline at four locations. The mean value of the strain in each of the four regions is plotted, and the error is quantified by means of an error bar indicating the spread of a single standard deviation of the strain measurement.

Examples of the first four strain measurements taken along the region of highest curvature of a 2 ply specimen are shown in Fig. 5. The horizontal axis shows the change in strain (expressed as a percentage). The vertical axis shows the distance in mm along the region of highest curvature from

the bottom edge to the top edge. The strain predicted by finite element analysis assuming a linear elastic orthotropic material is shown as a dotted line in Fig. 5 a.

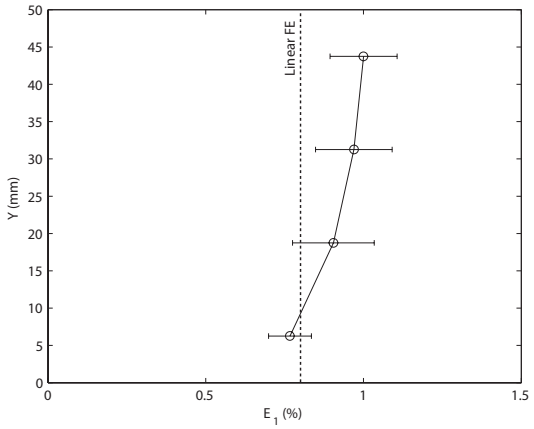

(a) Instantaneous strain (%)

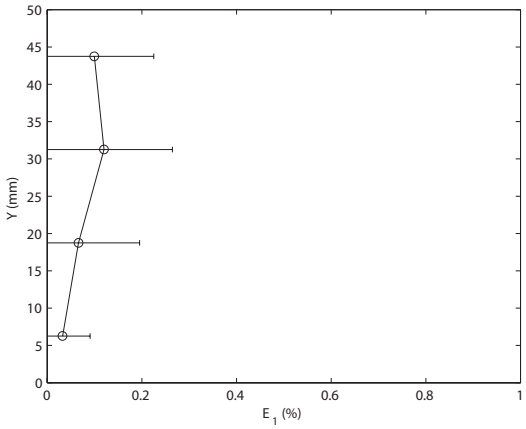

(b) Change in strain 0-21 days (%)

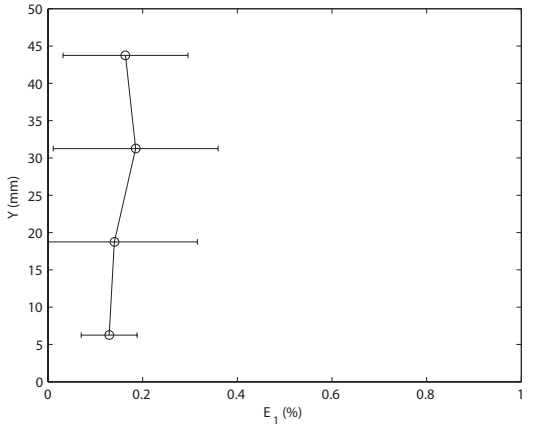

(c) Change in strain 21-27 days (%)

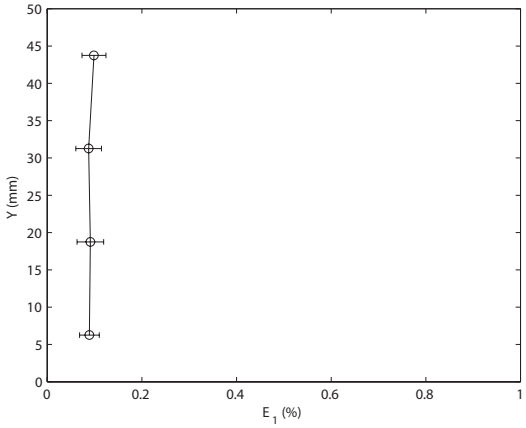

(d) Change in strain 27-33 days (%)

Figure 5: Measured principal strain changes on the line of highest curvature represented by the mean over four equal regions. Data is shown for the first 4 measurements tensile surface of a 2 ply IM7-8552 specimen.

It can be seen that the strain along the region of highest curvature is not constant, as predicted by finite element analysis, although the average value across the specimen is very close to the predicted value. This could be partly due to deviations from planarity in the experimental setup, but great care was taken to minimize this. A strong possibility is that it is the effect of strain redistribution due to immediate cracking. Further work, however, is needed to confirm this assumption. It has also been demonstrated by Murphey et al. [3] that specimen thickness varies significantly in local regions due to imperfect fiber distribution and regions of resin concentration. This is an additional extremely likely potential source of bending stiffness and hence surface strain variation.

The variation in measurement error, as indicated by the error bars, comes from two sources. In part it is due to the effect of small lighting differences in sequential images on the quality of the DIC. Inspection of Fig. 5 d, however, indicates that this effect is small. It is also indicative of the

large variation across the region of highest curvature due to variability in surface degradation or local specimen thickness.

There are two possibilities for evaluating the strain evolution using DIC: globally with reference to the original undeformed specimen configuration; locally/summatively with reference to the preceding configuration. The first approach is in principal the most accurate as it accounts for any nonlinearities in the strain field. However, the measurement noise already alluded to is found to be strongly amplified by differences in ambient conditions over long durations. The second approach is less susceptible to these errors and the accuracy and consistency of the measurement is found to be substantially improved. For this reason the second DIC approach is adopted, but it is important to convert the strains from Euler-Almansi form to percentage representation to carry out the summation. The assumption of small strains is implicit in this conversion, but this is acceptable as the changes in strain are indeed found to be small.

The evolution of the mean strain of the 2, 3, and 4-ply test specimens is plotted in Fig. 6. The horizontal axes show the time elapsed from the initial compression in days, and the vertical axes show the average current strain (expressed as a percentage). The error bars indicate the spread of a single standard deviation of the strain measurement at each time. This 'error' in part reflects the non-constant nature of the strain across the specimen – already observed in Fig. 5 a.

It can be seen that the finite element predictions, which are based on classical laminate theory, capture the instantaneous response of the 2 and 3-ply specimens well, but the 4-ply specimens are less well represented. This illustrates the limits of using thin shell theory to predict the behavior of composite compliant flexures. The limit of validity occurs between 3 and 4 plies of IM7-8552. This is an interesting result as it corresponds to the change in failure mode observed in the short term compression tests described in Sec. 2.3. The 3 ply specimens were observed to fail on the tensile surface, whereas the 4 ply specimens failed, as would be expected, on the compressive surface. In can be concluded that the increasing importance of through-thickness effects is a driver of this phenomenon.

For the strain evolution of all specimens a very similar global trend can be observed. From the instantaneous response, the strain in the tensile surface increases at a non-negligible, but steady rate. This is indicative of visco-elasto-plastic material behavior, possibly amplified by the evolution of fiber damage. After approximately 30 days however, the rate of change of strain in the tensile surface increases significantly. Global observation of the specimens does not indicate a significant change in geometry, so this behavior is indicative of a 'bursting' response in which the rate of individual fiber failures increases rapidly. This interpretation is backed up by the observation of surface damage evolution in Sec. 3.4 below. This indicates that in order to understand the behavior of compliant composite flexures it is necessary to consider their response on a microstructural in addition to a macro-structural scale.

It must be noted that typically, fiber response is linear to approximately 0.5% strain and increasingly nonlinear thereafter [3]. It can be seen that strains in the upper surface, even immediately after bending fall within this nonlinear region. This, in addition to the increasing importance of through-thickness effects, may account for the observed increasing discrepancy between the predicted linear response and the initial specimen behavior. Of course, the possibility also exists that any thickness variation effects, as alluded to above, may numerically cancel any nonlinearities resulting in a coincidental proximity to the linear response. Further work to carry out careful evaluation of the strain response at the fiber length scale would address this issue.

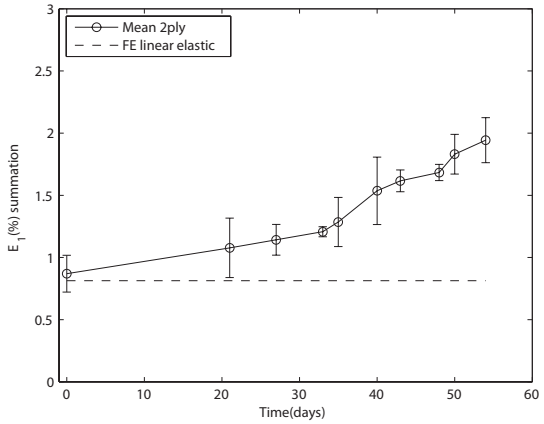

(a) 2 ply specimen principal strain evolution

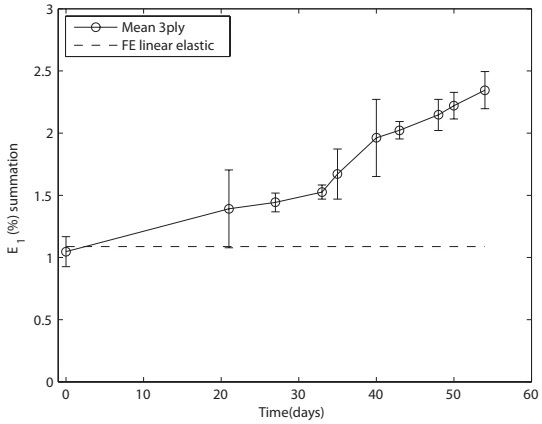

(b) 3 ply specimen principal strain evolution

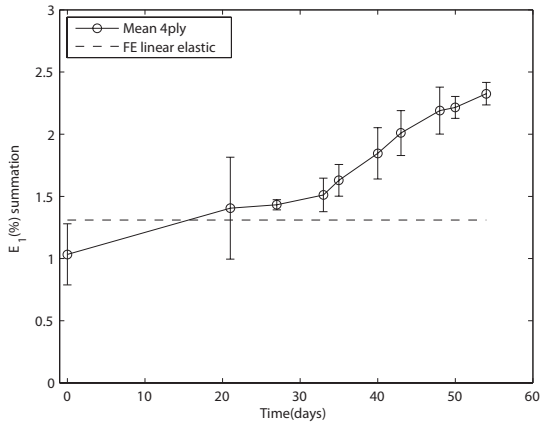

(c) 4 ply specimen principal strain evolution

Figure 6: Average principal strain evolution for all experimental specimens. Classical laminate theory finite element predictions assuming orthotropic linear elastic material properties are superposed for comparison.

3.4 Microscopy and Damage Evolution

Immediately after imaging for DIC measurement, the folded specimen is removed from the test rig and transported for visualization under a high power microscope. The specimen and locked compression platens (see interim report for details of the construction) are fixed to a machined angle section to ensure that it remains stably oriented during the microscopy. The magnified regions of highest curvature of the test specimens are photographed to enable comparison of the microstructure over the duration of the experiment. An example set of images showing the region of peak curvature of the tensile surface of a 4 ply specimen after 43 days is shown in Fig. 7. The sequence of images runs from the bottom edge (image 1) to the top edge (image 5). The edge damage visible in the top right hand corner of image 5 is an artifact of the specimen preparation and is not observed to contribute to the behavior of the specimen.

The microscope images are analyzed for the appearance of damage. This is partly a subjective

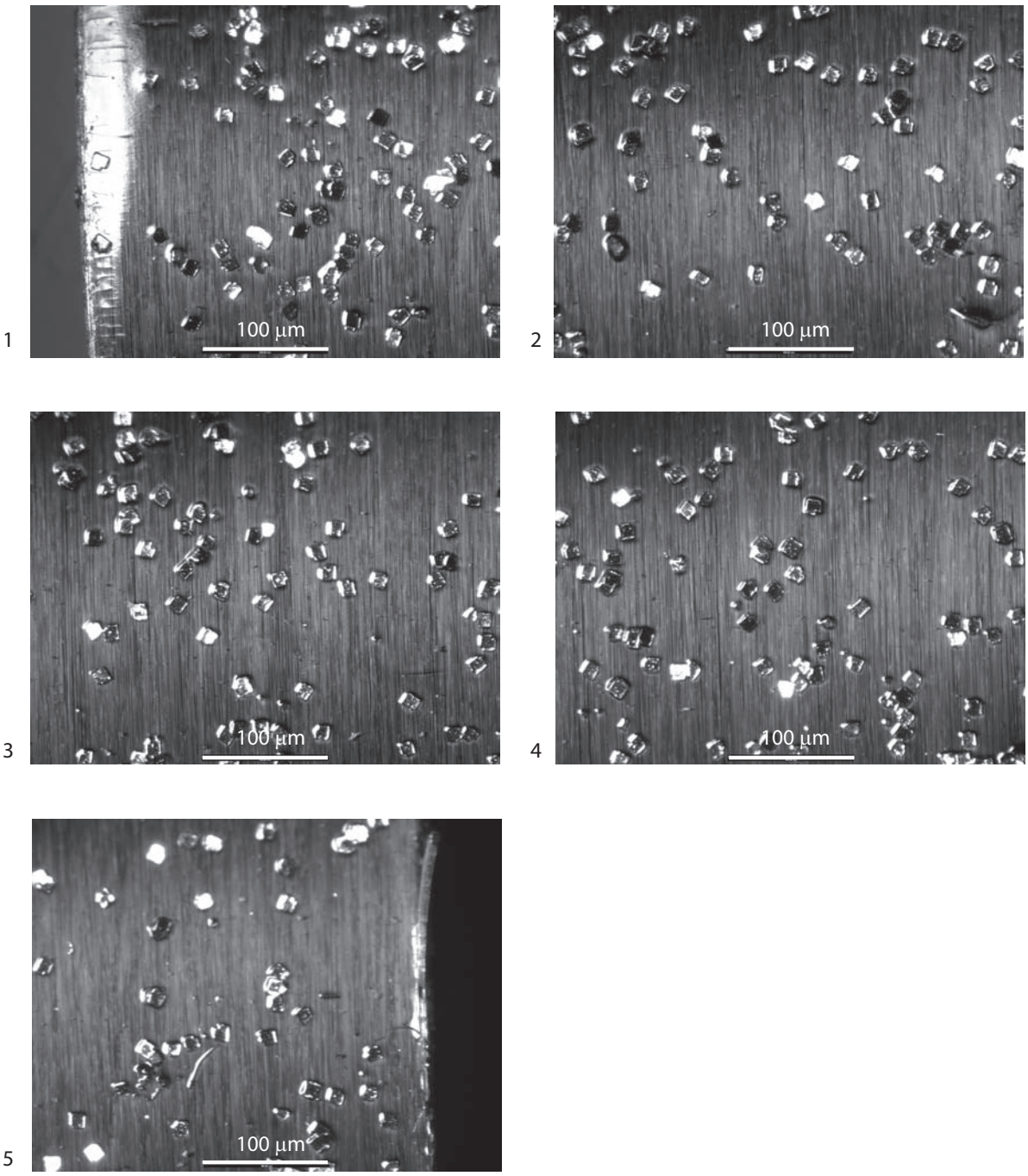

Figure 7: Example microscope images of deformed specimen. The sequence shows the region of highest curvature of the tensile surface of a 4 ply specimen after 43 days

process, but nonetheless provides an extremely useful indicator of the evolution of the specimen at a microstructural level. The method to determine the presence of damage is illustrated in Fig. 8. This shows the same region of the third 3-ply specimen 35 days (left hand side) and 40 days (right hand side) after initial compression. The damage occurs on a fiber length scale so it is necessary to magnify the images which leads to a corresponding loss of resolution. Correspondence between locations is confirmed by means of constellations formed from the specks of glitter which form the most recognizable landmark at this magnification. Clear damage can be seen in the right hand image centered on the top vertex of the constellation. This appears to be a crack in the fiber direction – the location is identified by the dotted ellipse.

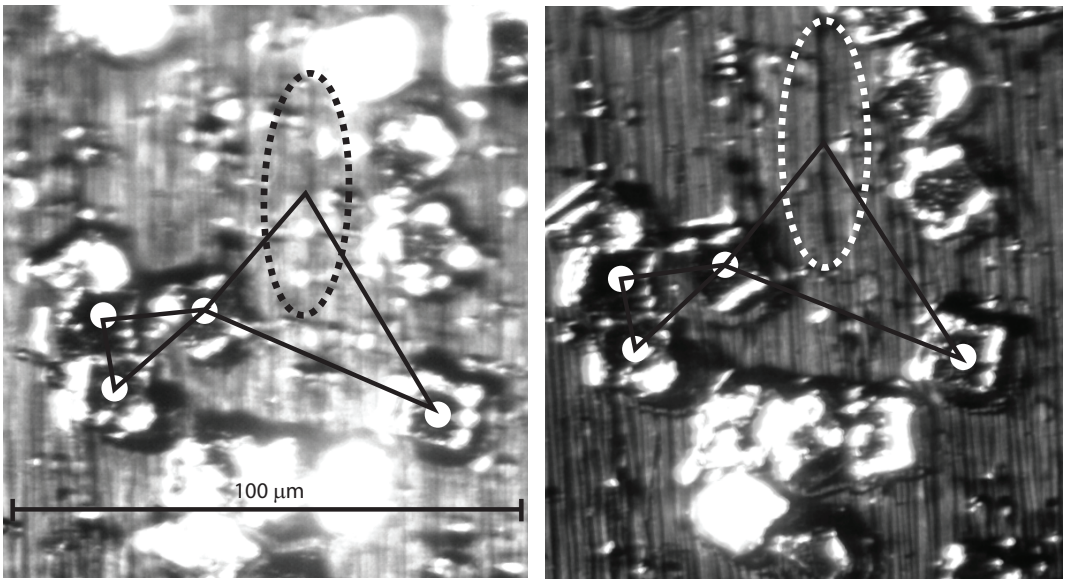

Figure 8: Illustration of image comparison to determine damage evolution. This shows the appearance of damage between 35 and 40 days after initial loading of the third 3-ply specimen.

The evaluation of whether or not significant damage has occurred in a region is subjective: each potential site must be assessed. In this case, the main indicator that damage has occurred comes from inspection of the region consisting of the intersection of the top triangle of the constellation and the damage site ellipse in the left hand image. It can be seen that glitter speckles are present in the region resulting in characteristic lens flare effects in the image. In the right hand image these speckles are clearly absent. This indicates that the damage – which may have been present in a lesser form in the left hand image – has increased to the extent that the speckles burst away from the specimen. Consequently the appearance of damage is recorded and plotted as described below. A similar process is repeated for all potential damage locations.

It was observed that damage consisted of three main types: minor surface damage – superficial resin cracks; highly-localized delamination regions; transverse cracks cutting fibres in the direction of principal strain. Of these types of failure, the first type is not recorded as it occurs across the whole surface and appears to be located entirely in the surface resin. The appearance of cases of the second type of failure is not recorded as it is an extremely rare event. Despite this, it is necessary to bare their existence in mind for future work.

The appearance of transverse cracks, however, are recorded and are plotted on schematic diagrams representing the region of highest curvature. Such diagrams illustrating the evolution of transverse

crack fiber damage in all nine test specimens are shown in Fig. 9. Each rectangle broadly corresponds to the specimen area shown in Fig. 7. N.B. as described above, the third 2 ply specimen failed after 21 days as a result of being subjected to further compression.

It can be seen that in general, although by no means uniquely, the damage occurring over the first 21 days is clustered at the top and bottom edges of the specimens. After this time, the frequency of damage is observed to increase, and the damage spreads towards the center of the highest-curved region. By the end of two months the damage is seen to be distributed across the entire region. This increase in damage frequency corresponds to the measured increase in strain shown in Fig. 6. This strongly supports the hypothesis that the increase in measured strain is due to a bursting effect in the fibers of the extreme surfaces.

It must be recognized that the subjective nature of the damage assessment will inevitably give rise to missed damage sites and false positive indications of damage. However, even accounting for this the trends described in the preceding paragraph are observed across all specimens, so the above conclusions may reasonably be drawn.

3.5 Experimental Program – Conclusions

It has been experimentally determined that the mean surface strains in all specimens increase from their instantaneous values, and at approximately 30 days after the initial compression the rate of strain increase, and the rate of observed damage, are both seen to grow. This is strongly indicative of IM7-8552 having a time-dependent material behavior with a characteristic time of the order of 30 days. It has also been determined that the strain varies across the surface of the specimens spatially as well as temporally. This is believed to be due to redistribution of deformation as a result of microstructural damage.

Although great care was taken to ensure repeatability of measurement conditions, it is believed that small differences in lighting conditions and resulting DIC errors are responsible for some of the measured strain variation across the specimen surfaces, in addition to localized damage. In future work, the experimental technique will be refined to reduce any such error.

The metallic paint speckles used to enable the macro-scale DIC are clearly visible in the images in Fig. 7. This raises the interesting question of the possibility of carrying out DIC images at the microscopic scale. This would enable an objective determination of the evolution of microscopic damage as opposed to the subjective, and time consuming, method described above.

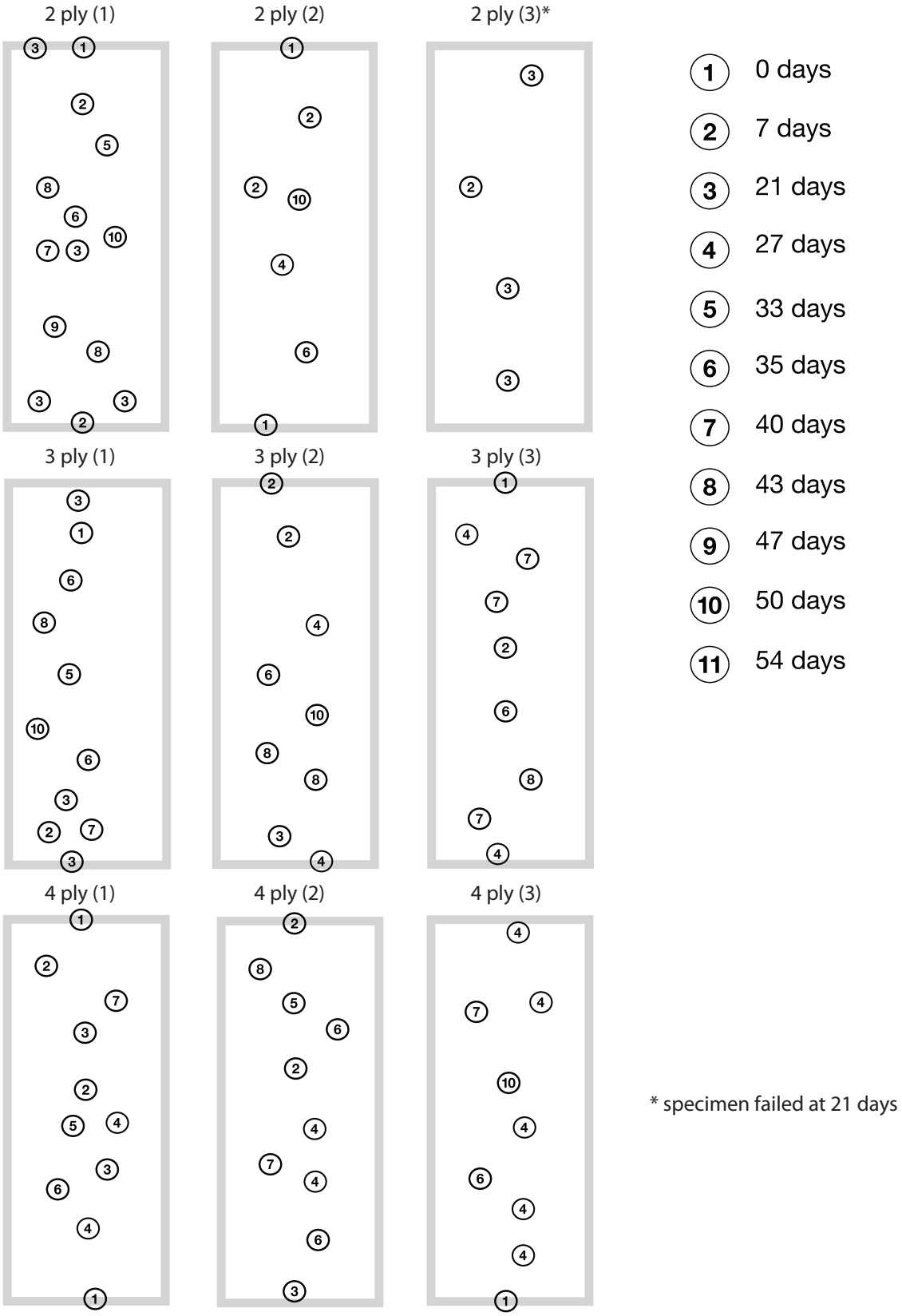

Figure 9: Schematic diagrams showing the time of appearance of crack damage in the region of highest curvature of all test specimens

4 Low Strain Rate Behavior of Compliant Flexures – Numerical Modelling

A primary goal of the long-term experimental testing is to provide information to enable the postulation of time-dependent material models which accurately characterize the behavior of the composite flexures. This will enable better prediction of the response of such flexures when they are held in a folded configuration for long durations.

The first stage in the numerical modelling of the composite specimens is to characterize the short-term linear elastic response. It has been demonstrated that an assumption of geometrically-nonlinear elasticity is an appropriate approximation for the flexures' behavior over durations that are small in comparison to the 'characteristic time' of the material. In order to model this behavior, it is assumed that the properties of the IM7-8552 specimens can be smeared to an orthotropic model using classical laminate theory (CLT). It is important to remember that the applicability of CLT is restricted to thin shells for which through-thickness effects can be ignored, particularly in the case of imposed large nonlinear out-of-plane deformation.

In the experimental test program it was noted that all of the specimens exhibited an increase in peak mean principal strain in the region of highest curvature. As already noted, this increase occurs over a region of time centered around approximately 30 days. The rate of increase is also observed to grow as time passes. Such behavior is not indicative of typical viscoelastic/plastic material behavior. However, a simple viscoelastic material model is nonetheless proposed for investigation. The purpose of this is to determine the global structural effect that results from such a material assumption and consequently what proportion of the observed behavior can be thus attributed. It is not expected at this stage to be able to capture the time-dependent behavior quantitatively, but a qualitative match still provides useful understanding.

The experimentally-observed evolution of the microscopic damage of the specimen surfaces indicates that a simple constitutive law may not be sufficient to characterize the long-term behavior fully. It is therefore necessary to incorporate the damage evolution into the material modelling. This is highly complex, and beyond the scope of the current program. However, some suggestions for appropriate approaches will be given.

In the remainder of this section, the focus will be on the implementation of the elastic and viscoelastic material models into the finite element analysis. Associated complexities with replicating the specimen loading environment will also be discussed.

4.1 Finite Element Modelling and Analysis

All finite element modelling is carried out using the commercial finite element package SAMCEF [5]. The composite flexures are modelled using first order quadratic shell elements formulated according to the Mindlin hypothesis. Individual plies are modelled and the shell properties are determined by means of classical laminate theory. The necessary element density is determined by means of a convergence test using the simulation of a linear elastic specimen in pure bending.

The compression rig platens are modelled as rigid surfaces. One is held stationary while the other is brought closer at a linear rate over 2 s to the required separation, resulting in the compression of the specimen. This asymmetric loading – adopted for ease of modelling – is representative of the short-term bending testing rather than the symmetric loading used in the long-term testing, but

E_{11}	171420	$(\mathrm{N/mm^2})$
E_{22}	9080	$(\mathrm{N/mm^2})$
G_{66}	5920	$(\mathrm{N/mm^2})$
ν_{12}	0.32	

Table 1: Orthotropic material properties for a single ply of IM7-8552

the difference in specimen response is negligible. Rigid contact is assumed between the compressing surfaces and the composite specimen.

In order to prevent numerical instabilities, a small pure bending moment is applied to the specimen to impart an initial curvature and govern the direction of specimen deflection. This moment is reduced to zero at a linear rate as the specimen is compressed. The analysis is carried out quasi-statically i.e. dynamic effects are neglected. The solver uses the Newmark algorithm with automatic time stepping.

The individual plies are modelled as linear elastic orthotropic laminae having the experimentally-determined properties of IM7-8552 uni-directional pre-preg. These properties are listed in Tab. 1. These linear elastic properties are also used as the unrelaxed (instantaneous) behavior of the viscoelastic material models. As an example of the analysis, the deformed configuration and the corresponding maximum principal strains of a linear elastic 2 ply specimen are shown in Fig. 10. As already seen, the resulting instantaneous maximum principal strains are plotted alongside the experimentally-determined results in Fig. 6.

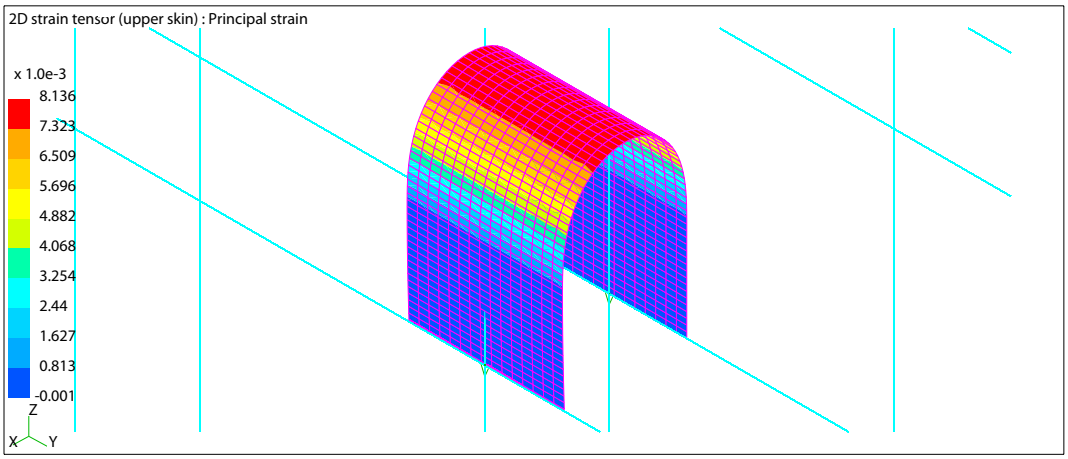

Figure 10: Finite element analysis showing the maximum principal strain on the tensile surface of a 2 ply specimen

4.2 Viscoelastic Material Hypothesis

One of the most simple time-dependent material models is the assumption of linear viscoelasticity [1]. A viscoelastic material is dissipative and depends on load rate in addition to magnitude. One way to model this is to represent the apparent decay in stiffness when a viscoelastic specimen is held under load by means of a series of decaying exponentials, also known as a Prony series.

For example, if a viscoelastic material is subjected to a step increase in strain ϵ which is then maintained, the resulting time-dependent stress $\sigma(t)$ may be represented by the Prony series

$$\sigma(t) = \frac{\partial W}{\partial \epsilon}\left(1 - \sum_i w_i \left(1 - e^{-t/\tau_i}\right)\right) \tag{6}$$

in which W is the strain energy, w_i are a set of weighting values, and τ_i are a set of characteristic times. After a time under load that is substantially greater than the largest characteristic time, the stress reaches an asymptotic value

$$\sigma_\infty = \frac{\partial W}{\partial \epsilon}\left(1 - \sum_i w_i\right) \tag{7}$$

This indicates that we can define a long term (relaxed) modulus E_∞ for a linear viscoelastic material, that is related to the short term (unrelaxed) modulus E_0 by

$$E_\infty = E_0\left(1 - \sum_i w_i\right) \tag{8}$$

The relaxation corresponding to each weight w_i will take place over the decade centered on the associated characteristic time τ_i.

A finite element analysis was carried out to determine whether such a viscoelastic material hypothesis could replicate the observed strain evolution behavior. A single term Prony series representation is sufficient to determine whether a qualitative match can be achieved so this was adopted. The trial material was specified with instantaneous (unrelaxed) linear-elastic orthotropic material properties as described above. The relaxation properties were specified with $w = 0.8$ (leading to an 80% reduction in stiffness and $\tau = 10.0$ s. This characteristic time is substantially smaller than the apparent characteristic time of ≈ 30 days observed in the experimental testing. However, this is unimportant: as already stated, the characteristic time centers the decade over which relaxation occurs. A smaller characteristic time substantially increases solution time and reduces computational memory requirements while its only effect is to shift the relaxation forward in time.

The viscoelastic time-dependent analysis was run, holding the location of the compression platens for a further 18 s after the initial deformation took place over 2 s. A characteristic time of $\tau = 10$ s means that the structure's response is essentially linear elastic over the initial folding period. The evolution of the principal strain in a centrally-located element in the region of highest curvature was monitored. It was found that the strain increased – as per experimental observation – but the change in value was minute (of the order 0.001%). This was confirmed by a convergence study to be a real effect and not a numerical error, but nonetheless it may be concluded that standard linear viscoelastic material behavior does not contribute significantly to the observed experimental response. This is an interesting outcome which indicates that the understanding of local damage evolution may be critical to the understanding of the flexures' long term behavior. It also indicates that any strain redistribution must be linked to the appearance of localized damage.

4.3 Numerical Modelling – Conclusions

The primary conclusion resulting from the numerical analysis is that a global material approach is insufficient to capture the complexities of the observed phenomena in the folded flexures. A

viscoelastic material model has been shown to have negligible effect on the global configuration of the specimen over time. This is confirmed by observation of the physical specimens. It has also been noted that, for the large out-of-plane distortion loading environment considered here, the assumption of thin shell mechanics implicit in classical laminate theory is applicable only for 2 and 3 ply specimens. A modelling approach which adequately accounts for through-thickness effects is clearly required.

It has been concluded in Sec. 3.4 that the increase in measured mean strain is strongly related to microstructural effects and the localized evolution of damage in the surface plies. This suggests that, to understand the behavior, it is necessary to account for micro-mechanical effects and to model the flexures at least at ply level. The damage evolution data – plotted in Fig. 9 – indicates that a stochastic approach to modelling the appearance of local damage may be appropriate. This is highly recommended for future studies.

5 General Conclusions

This program has successfully developed an experimental rig that enables the long term full-field strain measurement in the regions of maximum curvature of flexures in their deformed configuration. The measurement uses digital image correlation (DIC) techniques, and the rig permits concurrent testing of multiple specimens. This has enabled the long term response of composite flexures in bending to be recorded for the first time. Although only two-dimensional DIC has been used in this program, the rig is also configured for stereo (three-dimensional) measurement in future work if required.

The DIC measurements and microscopic observation have demonstrated that the long term behavior of composite flexures is strongly dominated by local microstructural effects. The strain profile varies across the specimen surfaces, but it has been shown that the mean value is still a useful performance metric. It has also been shown that the microscopic evolution of damage is correlated in time to the globally-observed increases in mean surface strain. Due to the substantial surface strain variation it is clearly desirable to improve the measurement accuracy further and remove any error associated with small variations in lighting between measurements.

It has been noted that the measured strain is affected by a number of factors including the possibility of redistribution due to local fiber damage, imperfections – particularly in thickness – of the test specimen, and fiber material nonlinearities. To further understanding, efforts should be made to decouple these effects. This could in part be achieved by initially loading the test specimens in pure bending as opposed to compression bending. However, it is considered that microscale investigation of individual fiber behavior is likely to be necessary to capture and fully understand the observed response.

The conclusions drawn from the experimental observations that an understanding of the microstructural behavior of flexures is key to the understanding of their global performance is confirmed by numerical analysis. It has been shown that an assumption of conventional time-dependent material properties in finite element analysis does not result in a replication of the observed response. An assumption of linear elastic orthotropic material properties has been shown to capture the instantaneous response of 2 and 3 ply specimens, but captures the immediate behavior of 4 ply specimens much less well. This indicates that it is necessary to account correctly for through-thickness effects. This provides an explanation for the observed failure phenomena in short-term compression testing of the flexures.

5.1 Future Work

As a result of this program, two promising lines of further enquiry, necessary to enable the long term structural performance of composite flexures have become apparent:

- ultra-accurate strain characterization at the fiber length scale;
- multi-scale numerical characterization accounting for microstructure, damage evolution, and stochastic effects.

The first would require DIC on images taken at the scale shown in Fig. 7. This is extremely challenging – specimen location repeatability, and appropriate speckle density are two of the major issues which must be addressed. Nonetheless, the objective assessment of damage evolution on the material surface would enable precise material characterization at a local scale and postulation of

stochastic parameters. This also enables systematic decoupling of effects due to strain redistribution due to damage, thickness variation, and fiber nonlinearities.

The second requires highly accurate numerical multi-scale modelling. It has been made apparent in the current test program that the local damage of fibers significantly affects the global response of the flexures. The multiple relevant length scales, the probabilistic nature of the damage evolution, and resolution in the long time scales appropriate to the problem, combine to result in a formidable computational challenge. However, such detailed characterization would enable the determination of 'smeared' global material models that would be appropriate for design purposes.

References

[1] Christensen, R. (1982) Theory of Viscoelasticity, 2nd ed. Academic Press Inc. New York

[2] Lava, P., Cooreman, S., Coppieters, S., De Strycker, M. and Debruyne D. (2009) Assessment of measuring errors in DIC using deformation fields generated by plastic FEA. *Opt. Las. Eng.,* 47, pp. 747-753

[3] Murphey, T., Sanford, G., and Grigoriev, M. (2011) Nonlinear Elastic Constitutive Modeling of Large Strains in Carbon Fiber Composite Flexures., In Proc. 16th International Conference on Composite Structures

[4] Pollard, E., Murphey, T. and Sanford, G. (2007) Experimental and Numerical Identification of a Monolithic Articulated Concentrated Strain Elastic Structure's (MACSES's) Properties, AIAA Paper No. AIAA 2007-2007, In proc. 48th AIAA/ASME/ASCE/AHS/ASC Structures, Structural Dynamics, and Materials Conference

[5] SAMCEF v12.0-03 Finite Element Package, Samtech S.A., Rue des Chasseurs-Ardennais, 8B-4031 Liège (Angleur), BELGIUM

[6] Sanford, G., Biskner, A., and Murphey, T. (2011) Large Strain Behavior of Thin Unidirectional Composite Flexures., AIAA Paper No. AIAA 2010-2698, In Proc. 51st AIAA/ASME/ASCE/AHS/ASC Structures, Structural Dynamics and Materials Conference

[7] Timoshenko, S. and Gere, J. (1961) Theory of Elastic Stability, 2nd ed. McGraw-Hill Book Company Inc. New York and London